Lattices for the lattice Boltzmann method

Shyam S. Chikatamarla*
LAV, Institute of Energy Technology, ETH Zurich, 8092 Zurich, Switzerland

Iliya V. Karlin†
LAV, Institute of Energy Technology, ETH Zurich, 8092 Zurich, Switzerland
and School of Engineering Sciences, University of Southampton, Southampton SO17 1BJ, United Kingdom
(Received 24 November 2008; published 1 April 2009)

A recently introduced theory of higher-order lattice Boltzmann models [Chikatamarla and Karlin, Phys. Rev. Lett. **97**, 190601 (2006)] is elaborated in detail. A general theory of the construction of lattice Boltzmann models as an approximation to the Boltzmann equation is presented. New lattices are found in all three dimensions and are classified according to their accuracy (degree of approximation of the Boltzmann equation). The numerical stability of these lattices is argued based on the entropy principle. The efficiency and accuracy of many new lattices are demonstrated via simulations in all three dimensions.

DOI: 10.1103/PhysRevE.79.046701 PACS number(s): 47.11.−j, 05.20.Dd

I. INTRODUCTION

The lattice Boltzmann (LB) method is a powerful new approach to hydrodynamics, with applications ranging from large Reynolds number flows to flows at the micrometer scale, porous media, and multiphase flows [1]. The LB method solves a fully discrete kinetic equation for populations $f_i(x,t)$, designed to reproduce the Navier-Stokes equations in the hydrodynamic limit. Populations correspond to discrete velocities c_i, $i=1,\ldots,n_d$, which fit into a regular spatial lattice with nodes x. This enables a simple and highly efficient "stream along links and equilibrate at nodes" realization of the LB algorithm.

In order to establish a LB model, it is crucial to choose the right set of discrete velocities c_i, their corresponding weights W_i, and a reference temperature T_0. In one dimension, the simplest choice of discrete velocities c_i is $\{0,\pm 1\}$ [the one-dimensional three-velocity (D1Q3) lattice]. For this simple lattice, the derivation of weights and the reference temperature are well known [2–4]. In higher dimensions, the D1Q3 lattice manifests itself—via a tensor product of D copies of D1Q3—as the well-known D2Q9 lattice in 2D and the D3Q27 lattice in 3D (and its prunes, the D3Q15 and D3Q19 lattices). A majority of the LB models and simulations to date have used these standard lattices. Here, we follow the established nomenclature, and label the models as DnQk, where n is the dimension of space, and k is the number of discrete velocities.

However, the three-velocity lattice and its counterparts in higher dimensions suffer from incomplete Galilean invariance [5–7]. That is, the Navier-Stokes equations for density and momentum are not fully recovered by the LB equation on these lattices. Also, for further applications such as compressible flows [8], multiphase flows [9], multicomponent flows [10], or microflows [11], more accurate and isotropic lattices become important. Hence, a concrete effort is required in establishing higher-order lattices for lattice Boltzmann methods.

To improve the accuracy and isotropy of a lattice, a larger number of discrete velocities is required. One way of obtaining higher-order LB models is by discretizing the Boltzmann equation on the roots of Hermite polynomials [6,12]. This route of higher-order Gauss-Hermite quadratures promised a systematic derivation of new complete Galilean-invariant LB models [6,12]. However, since the roots of Hermite polynomials are *irrational*, the corresponding discrete velocities cannot be fitted into a regular space-filling lattice. Thus, one of the most important advantages of the LB methods, the exact space discretization of the advection step, is lost with the Gauss-Hermite quadrature-based off-lattice models. Although in our construction the off-lattice Gauss-Hermite-based mdoels are derived as limiting case solutions, we shall focus here on the genuine lattice-based or integer-valued discrete-velocity models.

For the three-velocity set, the derivation of a lattice Boltzmann scheme has been achieved in several different ways [2–4]. However, none of these approaches enabled a systematic construction of larger (integer-valued) velocity sets which would better approximate Boltzmann's kinetic theory. More importantly, none of these theories could claim that the construction would lead to a stable numerical scheme; most of the earlier attempts remained a process of trial and error [13–15]. In particular, the approach of [14,15] is based on a quadrature representation of the equilibrium moments (not necessarily Gauss-Hermite) where the nodes of the quadrature are chosen empirically in such a way as to reflect higher-order isotropy.

In a recent Letter [7], we have introduced a systematic approach to constructing higher-order lattices suitable for stable LB models. We continue here with the entropic approach which promises to be a viable candidate for the construction of higher-order lattices for lattice Boltzmann methods [7]. The construction first proceeds in one dimension and is then extended to two and three dimensions. The theory presented is general in nature; the standard lattices used in LB simulations follow as low-order approximations in this construction.

*shyam_css@yahoo.com
†karlin@lav.mavt.ethz.ch

FIG. 1. One-dimensional four-velocity set.

The outline of the paper is as follows. In Sec. II, for the sake of completeness, we review the entropic construction of Ref. [7] in one spatial dimension. Entropy functions and the reference temperatures are found for all four- and five-velocity sets (Sec. II A), together with the expressions for the equilibrium populations. The higher-order lattices with seven and nine velocities are presented in Appendixes C and D, respectively. We further discuss the order of isotropy of the lattice approximation (Sec. II B). We demonstrate with a numerical example that the lattices which do not support the entropy function are unstable, unlike the admissible lattices (Sec. II C). Also, in Appendix B we demonstrate that higher-order lattices host several nontrivial LB models with Gaussian-like and non-Gaussian equilibria.

In Sec. III, we generalize the one-dimensional lattices of Sec. II to two and three spatial dimensions. The general method of generating the higher-dimensional lattices from any of the one-dimensional velocity sets of Sec. II, is described in Sec. III A, whereas the one-dimensional five-velocity set $\{0,\pm1,\pm3\}$ is used in the following. The two-dimensional D2Q25 lattice with 25 velocities per grid point is fully described and validated numerically in Sec. III C, and its three-dimensional counterpart, the D3Q125 lattice, in Sec. III D. It is argued that the accuracy of the higher-order lattices in two and three dimensions is the same as their generating one-dimensional lattice.

A systematic procedure of pruning (reducing the number of discrete velocities) is presented in Sec. IV. The pruning procedure enables to significantly reduce the number of discrete velocities in three dimensions. The particularly important D3Q41 lattice as a prune of the D3Q125 lattice is described in detail. In Sec. V, the D3Q41 LB model is validated with the three-dimensional Taylor-Green vortex flow simulation, and results are found in good agreement with the available direct numerical simulation of the incompressible Navier-Stokes equation using a spectral element code. Finally, the discussions are presented in Sec. VI.

II. LATTICE BOLTZMANN HIERARCHY IN ONE DIMENSION

A. Entropic construction

Moving on from the D1Q3 lattice with velocities $\{0,\pm1\}$, we shall now search systematically for *all* possible discrete velocity sets, in one dimension, whose equilibria better approximate the higher-order moments of the local Maxwellian. Let us list the first few moments of the Maxwellian at a fixed reference temperature T_0, realized as sums over a finite number of velocities n_d,

$$\rho=\sum_{i=1}^{n_d} f_i^{\mathrm{eq}},\quad \rho u=\sum_{i=1}^{n_d} f_i^{\mathrm{eq}} c_i,$$

$$P^{\mathrm{eq}}=\sum_{i=1}^{n_d} f_i^{\mathrm{eq}} c_i^2=\rho T_0+\rho u^2,$$

$$Q^{\mathrm{eq}}=\sum_{i=1}^{n_d} f_i^{\mathrm{eq}} c_i^3=3\rho T_0 u+\underline{\rho u^3},$$

$$R^{\mathrm{eq}}=\sum_{i=1}^{n_d} f_i^{\mathrm{eq}} c_i^4=3\rho T_0^2+\underline{6\rho T_0 u^2+\rho u^4}. \tag{1}$$

Here the density ρ and the momentum density ρu are the locally conserved quantities, and T_0 is the reference temperature, related to the speed of sound as $T_0=c_s^2$. The second-, third-, and fourth-order moments P, Q, and R are interpreted as the pressure tensor, the energy flux, and the rate of change of the energy flux, respectively. Their values at the discrete velocity equilibrium presented in Eq. (1) correspond to the well-known Maxwell-Boltzmann (MB) relations.

Our task now is to search for discrete velocity sets whose equilibrium approximates, as closely as possible, the MB relations (1). Note that the moments of the equilibrium of the three-velocity set $\{0,\pm1\}$ (and its extensions in higher dimensions) deviate from the MB relations (1). In particular, the underlined terms in Eq. (1) are not correctly recovered (see Appendix A for further details on the accuracy of the D2Q9 lattice).

Before we proceed with the derivation of higher-order lattices, let us recall the entropic construction [2,12,16] of the LB models. In the entropic construction, the equilibrium populations f_i^{eq} minimize the entropy function H,

$$H=\sum_{i=1}^{n_d} f_i \ln\left(\frac{f_i}{W_i}\right), \tag{2}$$

with appropriately chosen weights $W_i>0$, under the constraints of mass and momentum conservation, $\Sigma_{i=1}^{n_d}\{1,c_i\}f_i^{\mathrm{eq}}=\{\rho,\rho u\}$. Once the equilibrium distribution is known, a lattice Bhatnagar-Gross-Krook (LBGK) scheme can be set up,

$$f_i(x+c_i,t+1)-f_i(x,t)=\frac{2}{2\tau+1}[f_i^{\mathrm{eq}}(x,t)-f_i(x,t)], \tag{3}$$

where τ is related to the kinematic viscosity ν as $\nu=\tau c_s^2$. This simple construction ensures thermodynamic consistency and stability. Further enhancement of stability can be achieved by employing the entropic time-stepping instead of the standard LB time steps [2,17]. In this paper we do not dwell on the latter stabilization procedure and use the LBGK model (3).

The first generic extension of the D1Q3 lattice, $\{0,\pm1\}$, is the four-velocity set $\{\pm m,\pm n\}$ ($n_d=4$; see Fig. 1). At this stage of the analysis, we do not enforce the values of m and n to be integer. Our goal is to derive the weights $W_{\pm m}$, $W_{\pm n}$, and the reference temperature $T_0(m,n)$, at which the resulting equilibrium implies the constitutive relations for the pressure tensor P^{eq} and the energy flux Q^{eq} (1).

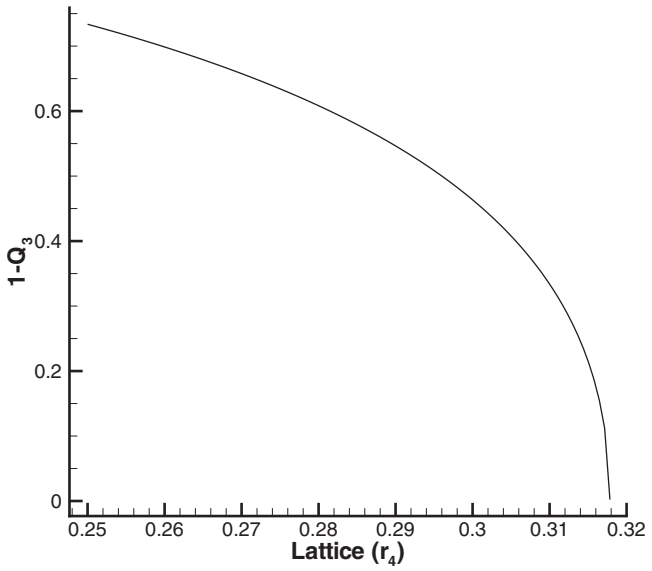

FIG. 2. Error in the equilibrium energy flux $1-Q_3^{\mathrm{eq}}(r_4)$ for all admissible four-velocity sets.

Using a series expansion in powers of velocity u, in order to obtain f_i^{eq} from the minimization problem (entropic construction), we find that the zeroth-, the first-, and the second-order terms (1) are recovered with the following weights and reference temperature [7]:

$$W_{\pm m}=\frac{m^2-5n^2+\sqrt{m^4-10n^2m^2+n^4}}{12(m^2-n^2)},$$

$$W_{\pm n}=\frac{5m^2-n^2-\sqrt{m^4-10n^2m^2+n^4}}{12(m^2-n^2)},$$

$$T_0=\frac{m^2+n^2+\sqrt{m^4-10n^2m^2+n^4}}{6}. \tag{4}$$

At this point we are left with just one degree of freedom—the ratio between the velocities, $r_4(m,n)=m/n$. The ratio r_4 needs to be chosen without violating the positivity of either the weights or the reference temperature. From (4), it follows that any $r_4 \leqslant r_4^*$ $(r_4^*=\sqrt{3}-\sqrt{2})$ satisfies the positivity requirement. The limiting ratio r_4^* is related to the roots of the Hermite polynomials and the popular Gauss-Hermite quadrature used in the LB literature [7].

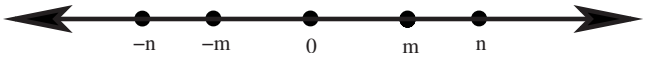

FIG. 3. One-dimensional five-velocity set.

Fixing this ratio at $r_4=r_4^*$, one obtains an off-lattice velocity set identical to the one obtained using the Gauss-Hermite quadrature. At this value r_4^*, the cubic term in the equilibrium energy flux, $Q^{\mathrm{eq}}=3\rho T_0 u+Q_3^{\mathrm{eq}}(r_4)\rho u^3$, becomes the same as in the Maxwell-Boltzmann relation, viz., $Q_3^{\mathrm{eq}}(r_4^*)=1$ (complete Galilean invariance). However, we are now free to choose the ratio $r_4 \leqslant r_4^*$ such that m and n are integers. This enables us to set up a LB scheme with integer-valued velocities. Moreover, this particular analysis gives us an insight into the accuracy of all possible four-velocity sets. It can be seen in Fig. 2 that deviation of the energy flux from the Maxwell-Boltzmann relation monotonically vanishes as r_4 approaches r_4^*. Thus, we have classified all the four-velocity sets according to their accuracy.

It was earlier conjectured that the rest population, corresponding to $c_i=0$, plays an important role in obtaining a stable LB scheme [13]. Contrary to this, all the four-velocity sets derived herein do not contain a rest population and yet are numerically stable. Test simulations were carried out for the one-dimensional shock tube problem (Sec. II C), and all the four-velocity lattices described herein were found to be numerically stable. However, the advantages over the three-velocity set are not very significant due to the fact that none of the (integer-valued) four-velocity sets are completely Galilean invariant ($Q_3^{\mathrm{eq}}=1$ only at the limit $r_4=r_4^*$). Thus, we continue our construction further toward more accurate lattices and with more discrete velocities.

For a generic five-velocity set $\{0,\pm m,\pm n\}$, we have one more degree of freedom when finding the corresponding weights (see Fig. 3). We are now free to choose independent weights for the three discrete velocities, and the value of the reference temperature. Proceeding with the derivation of the equilibrium as in the four-velocity case, we obtain the weights and the reference temperature as

$$W_0=\frac{-3m^4-3n^4+54m^2n^2+(m^2+n^2)\sqrt{9m^4-42n^2m^2+9n^4}}{75m^2n^2},$$

$$W_{\pm m}=\frac{9m^4-6n^4-27n^2m^2-(3m^2-2n^2)\sqrt{9m^4-42n^2m^2+9n^4}}{300m^2(m^2-n^2)},$$

$$W_{\pm n}=\frac{9n^4-6m^4-27n^2m^2-(3n^2-2m^2)\sqrt{9m^4-42n^2m^2+9n^4}}{300n^2(n^2-m^2)},$$

$$T_0=\frac{3m^2+3n^2-\sqrt{9m^4-42n^2m^2+9n^4}}{30}. \tag{5}$$

TABLE I. Lattice Boltzmann (LB) models as rational-number approximations to roots of Hermite polynomials. Rows are grouped according to the number of discrete velocities, n, from 3 to 5 (levels). The case $n=3$ corresponds to the standard LB model. Three first integer-valued LB velocity sets, corresponding to the smallest values $m=1,2,3$, are given for the fourth and the fifth levels. Roots of Hermite polynomials $\mathcal{H}_n$ are given in the last row of each n level. Coefficients of the constitutive relations (7) corresponding to the four- and five-velocity LB models are presented. The Maxwell-Boltzmann coefficients are given in the last row for comparison. The last column gives the ratios between the magnitudes of the discrete velocities.

n	Model	c_i	P_4	Q_3	R_2	R_4	$r=m/n$
3	LB	$0,\pm 1$	$-\frac{4}{3}$	0	3	$-\frac{4}{3}$	
3	$\mathcal{H}_3$	$0,\pm\sqrt{3}$	$-\frac{4}{3}$	0	3	$-\frac{4}{3}$	
4	LB	$\pm 1,\pm 4$	−0.041	0.266	3.799	−0.697	0.25000
4	LB	$\pm 2,\pm 7$	−0.012	0.425	4.275	−0.614	0.28571
4	LB	$\pm 3,\pm 10$	−0.005	0.536	4.610	−0.534	0.30000
4	$\mathcal{H}_4$	$\pm\sqrt{3\pm\sqrt{6}}$	0	1	6	0	0.31738
5	LB	$0,\pm 1,\pm 3$	0	1	6	0.031	0.33333
5	LB	$0,\pm 2,\pm 5$	0	1	6	0.218	0.40000
5	LB	$0,\pm 3,\pm 7$	0	1	6	0.345	0.42857
5	$\mathcal{H}_5$	$0,\pm\sqrt{5\pm\sqrt{10}}$	0	1	6	1	0.47449
∞	MB	continuous	0	1	6	1	

The equilibrium energy flux Q^{eq} can now be set in full agreement with the Maxwell-Boltzmann value (1) for all the five-velocity sets, while the fourth-order moment R^{eq} is recovered up to the quadratic term $(6\rho T_0 u^2)$,

$$R^{\mathrm{eq}} = 3\rho T_0^2 + 6\rho T_0 u^2 + R_4(r_5)\rho u^4. \tag{6}$$

The fourth-order term $R_4(r_5)\rho u^4$ depends on the ratio of the velocities $r_5=m/n$. Again, the Maxwell-Boltzmann value $R_4=1$ is obtained when r_5 reaches the limit value $r_5^*=(\sqrt{5}-\sqrt{2})/\sqrt{3}$. The ratio r_5^* is equal to the ratio of the nontrivial roots of the fifth-order Hermite polynomial. A monotonic convergence is observed also in the case of five-velocity sets. This completes the classification of all the five-velocity sets. As mentioned above, all the five-velocity sets have a useful feature, viz., the Maxwell-Boltzmann form of the equilibrium energy flux Q^{eq} is fully recovered, which makes the corresponding LB models completely Galilean invariant (they recover isothermal Navier-Stokes equations).

In order to realize a *lattice* Boltzmann scheme we need integer-valued velocities m and n, because, for non-integer-valued (or non-space-filling) lattices, the advection step of the LBGK equation (3) cannot be discretized *exactly*. For non-integer-valued discrete velocities, like the ones obtained from the Gauss-Hermite quadrature, we need to use interpolation schemes in order to complete the advection step. This takes away one of the primary advantages of LB methods. Interpolation on slowly varying fields like density, velocity, temperature, etc. is different from interpolating the populations themselves. The populations in a LB scheme are functions of the basic fields and their higher-order derivatives, for example, the Chapman-Enskog approximation to the populations [18]. Hence, simple low-order interpolation schemes may not be sufficient in order to accurately advect the populations, thereby leading to numerical dissipation.

Due to the generic nature of the construction we have followed so far, lattices with arbitrary m and n have been identified. We can now choose m and n to be integers and establish a lattice scheme. We see that, strikingly and non-trivially, some seemingly obvious lattices are immediately ruled out. In particular, the first admissible four-velocity set is $\{\pm 1,\pm 4\}$, that is, for example, the set $\{\pm 1,\pm 2\}$ is prohibited. Indeed, for the $\{\pm 1,\pm 2\}$ lattice, the ratio of the velocities is $0.5>r_4^*$, and the reference temperature $T_0(1,2)$ (4) does not exist (is complex valued). For the same reason, a popular five-velocity lattice $\{0,\pm 1,\pm 2\}$ is also ruled out $(0.5>r_5^*)$. This explains why earlier attempts to construct a LB model on this lattice failed to produce a numerically stable scheme (see Sec. II C).

In Table I some of the admissible lattices that we have constructed so far are presented. For these lattices, closeness of the moments to the Maxwell-Boltzmann moments is indicated through the coefficients of the terms appearing in the MB relations (1). For example, P_n refers to the coefficient of the term u^n in the second-order equilibrium moment P^{eq}; similarly Q_n and R_n:

$$P^{\mathrm{eq}} = \rho T_0 + \rho u^2 + P_4\rho u^4,$$

$$Q^{\mathrm{eq}} = 3\rho T_0 u + Q_3\rho u^3,$$

$$R^{\mathrm{eq}} = 3\rho T_0^2 + R_2\rho T_0 u^2 + R_4\rho u^4. \tag{7}$$

Two important conclusions can be drawn from Table I. First, the quality of the reconstruction of the moments *monotonically* depends on the closeness of the ratio $r(m,n)$ to the corresponding limit (Hermite) value. As $r_4(m,n)\to r_4^*$, the corresponding coefficients Q_3, R_2, and P_4 tend monotonically to the values corresponding to the model based on the fourth-order Hermite polynomial $\mathcal{H}_4$. In the same way, the coefficient R_4 tends to 1 as $r_5(m,n)\to r_5^*$, thus accomplishing

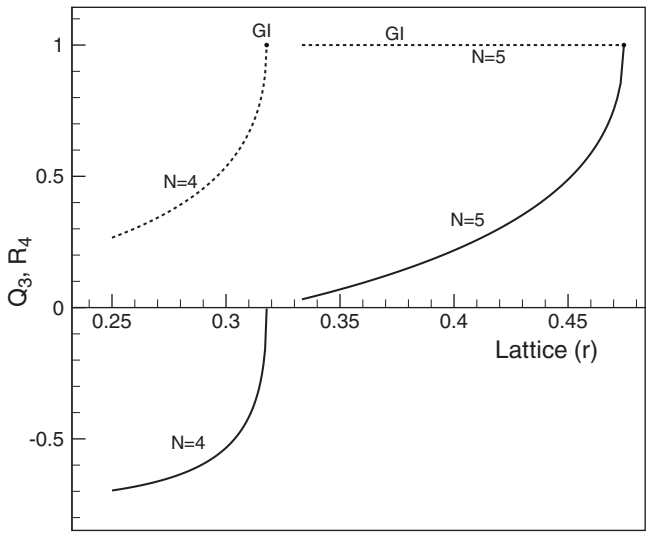

FIG. 4. Convergence of moments for the four- and five-velocity sets. Functions $Q_3(r)$ (dashed lines) and $R_4(r)$ (solid lines) are shown for all admissible four- and five-velocity sets. Completely Galilean-invariant isothermal models correspond to $Q_3=1$.

the full reconstruction of all the relevant moments in the Maxwell-Boltzmann form. Second, switching to the next higher number of discrete velocities (from n_d to n_d+1), one does not spoil the quality already reached at the n_d level. Indeed, the Maxwell-Boltzmann values $Q_3=1$, $R_2=6$, and $P_4=0$, which are recovered by the four-velocity LB approximations in the limit $r_4 \to r_4^*$, all remain intact for the five velocity sets; only the remaining coefficient R_4 is monotonically improved (see also Fig. 4). In other words, all the five-velocity LB models given in Table I are completely Galilean invariant. While this is expected for the models based on the Gauss-Hermite quadrature, the fact that the same is true also for the rational-number lattice Boltzmann approximations is nontrivial.

Thus, with the integer-valued velocities of Table I, and the corresponding expressions for the weights, we set up the lattice equilibria f_i^{eq} as minima of the entropy (2) (f_i^{eq} are easily derived by solving the minimization problem by perturbation in powers of u), and hence the lattice BGK models. All these lattices are based on the entropy function (2), and are thermodynamically consistent and numerically stable. The $\{0, \pm 1, \pm 3\}$ five-velocity set, in particular, has a number of advantages over the three-velocity set $\{0, \pm 1\}$ due to the correctness of the equilibrium energy flux Q^{eq}. This zero-one-three (ZOT) lattice will serve as a basis for higher-dimensional generalizations below (see Sec. III). The accuracy of the equilibrium moments of the ZOT lattice is as follows:

$$P^{\mathrm{eq}} = \rho T_0 + \rho u^2 + O(u^6),$$

$$Q^{\mathrm{eq}} = 3\rho T_0 u + \rho u^3 + O(u^5),$$

$$R^{\mathrm{eq}} = 3\rho T_0^2 + 6\rho T_0 u^2 + O(u^4). \tag{8}$$

The family of lattices based on the ZOT lattice can possibly replace the family of standard lattices based on the D1Q3 three-velocity lattices used so far in a majority of LB simulations.

Let us continue the entropic construction further toward more accurate lattices. We skip the six-velocity set and move on to the seven-velocity sets. Without any loss of generality, a seven-velocity set can be represented as $\{0, \pm 1, \pm n, \pm m\}$. The entropic construction proceeds in the same fashion as for the four- and the five-velocity sets. The general expressions for all seven-velocity sets are given in Appendix C. Let us denote by $c_{\max}=\max_{i=1,\ldots,n_d}|c_i|$ the maximal absolute value of the velocity in a given discrete-velocity set. We call the velocity set the shortest lattice in a family of admissible lattices with a given number of the velocities n_d if the minimal value of $c_{\max}$ is attained by this lattice. For example, the ZOT lattice is the shortest in the family of admissible five-velocity sets (see Table I). The shortest lattice in the seven-velocity family is the set $\{0, \pm 1, \pm 2, \pm 3\}$, the weights and reference temperature for which are

$$W_0 = \frac{1}{36}\{T_0[3(14-5T_0)T_0-49]+36\},$$

$$W_{\pm 1} = \frac{1}{16}T_0[T_0(5T_0-13)+12],$$

$$W_{\pm 2} = \frac{1}{40}T_0[5(2-T_0)T_0-3],$$

$$W_{\pm 3} = \frac{1}{720}T_0[15(T_0-1)T_0+4],$$

$$T_0 = \frac{2}{3} + \frac{1}{3}\sqrt[3]{\frac{7}{5(3\sqrt{30}-5)}} - \frac{\sqrt[3]{\frac{1}{7}(-5+3\sqrt{30})}}{35^{2/3}}$$

$$\approx 0.697\,953\,322\,019\,683\,1. \tag{9}$$

The accuracy of the moment reconstruction on the $\{0, \pm 1, \pm 2, \pm 3\}$ lattice is

$$P^{\mathrm{eq}} = \rho T_0 + \rho u^2 + O(u^8),$$

$$Q^{\mathrm{eq}} = 3\rho T_0 u + \rho u^3 + O(u^7),$$

$$R^{\mathrm{eq}} = 3\rho T_0^2 + 6\rho T_0 u^2 + \rho u^4 + O(u^6). \tag{10}$$

Comparing this with the result for the ZOT lattice (8), we see that the fourth-order moment R^{eq} is matched, and the accuracy for the moments P^{eq} and Q^{eq} is two orders of magnitude higher with the shortest D1Q7 lattice (the same holds also for all other admissible lattices of the seven-velocity family; see Appendix C). The D1Q9 lattices are also presented in Appendix D.

B. Order of isotropy φ

It can be seen from the above construction that extending the velocity set leads not only to matching moments of in-

creasingly higher order but also to the improvement of the order of errors in the lower-order moments. For example, in the case of the seven-velocity lattices, the second-order moment P^{eq} is recovered with $O(u^8)$ errors, the third-order moment with $O(u^7)$ errors, and the fourth-order moment with $O(u^6)$ errors. In other words, the order of the moment plus the order of accuracy with which it recovers the corresponding Maxwell-Boltzmann relation remains the same for various moments.

In order to quantify this observation, let us denote M_p^{eq}, where $p \geqslant 2$, the generic higher-order equilibrium moment $M_p^{\mathrm{eq}} = \Sigma_{i=1}^{n_d} f_i^{\mathrm{eq}} c_i^p$ (that is, $P^{\mathrm{eq}} = M_2^{\mathrm{eq}}$, $Q^{\mathrm{eq}} = M_3^{\mathrm{eq}}$, and so on). Any moment M_p^{eq} can be represented as an expansion into powers of the velocity u,

$$M_p^{\mathrm{eq}} = \sum_{q=0}^{\infty} a_{pq} u^q. \tag{11}$$

The moments of the same order of the local Maxwellian, M_p^{MB}, are polynomials of the order p,

$$M_p^{\mathrm{MB}} = \sum_{q=0}^{p} a_{pq}^{\mathrm{MB}} u^q. \tag{12}$$

For a given discrete-velocity equilibrium, we say that the Maxwell-Boltzmann form of the moment M_p^{eq} is recovered with accuracy of order k if the first nonvanishing coefficient of the expansion

$$M_p^{\mathrm{eq}} - M_p^{\mathrm{MB}} = \sum_{q=0}^{\infty} (a_{pq} - a_{pq}^{\mathrm{MB}}) u^q, \tag{13}$$

corresponds to the term of the order u^k. With these definitions, for each higher-order moment we introduce a function of two integer variables, $\varphi(p,k)$, given by the sum of the order of the moment $p \geqslant 2$ and order of accuracy for that moment, $k \geqslant 0$,

$$\varphi_{pk} = p + k. \tag{14}$$

The entropic construction of the lattices above demonstrates monotonicity in the following sense. The value of the function φ_{pk} is constant for all the corresponding (independent) equilibrium moments M_p^{eq} with p varying from $p=2$ to n_d, where n_d is the number of discrete velocities (for a set with n_d discrete velocities only n_d moments have independent dynamics, while the higher moments are permanently slaved). This single value φ is the unique characteristic accuracy of all the moments of a given lattice, and therefore characterizes the lattice itself (below, we refer to this value as the order of isotropy φ).

For the standard D1Q3 lattice, we have $\varphi=6$; i.e., the equilibrium pressure tensor ($p=2$) has errors of order $O(u^4)$ ($k=4$), the equilibrium energy flux ($p=3$) has errors of order $O(u^3)$, the fourth-order moment has errors of order $O(u^2)$, etc. Similarly, all the admissible integer-valued four-velocity lattices have $\varphi=7$, the five-velocity lattices D1Q5 have $\varphi=8$, the seven-velocity lattices have $\varphi=10$. We say that the Maxwell-Boltzmann equilibrium relation for the equilibrium moment M_p^{eq} is *fully recovered* if the first nonvanishing term in Eq. (13) is of order $O(u^{p+1})$ or higher ($k > p$). In view of the monotonicity in the entropic construction, the full recovery of a moment also implies the full recovery of all the lower-order moments. Figure 5 shows how various discrete velocity sets recover the Maxwell-Boltzmann relations. The highest moment that is fully recovered, $p_{\max}$, varies from $p_{\max}=2$ for the D1Q3 lattice to $p_{\max}=4$ for the D1Q7 lattice. Note that the latter is the lowest-order lattice which fully recovers the Maxwell-Boltzmann relations to the order required for constructing LB models for fully compressible flows.

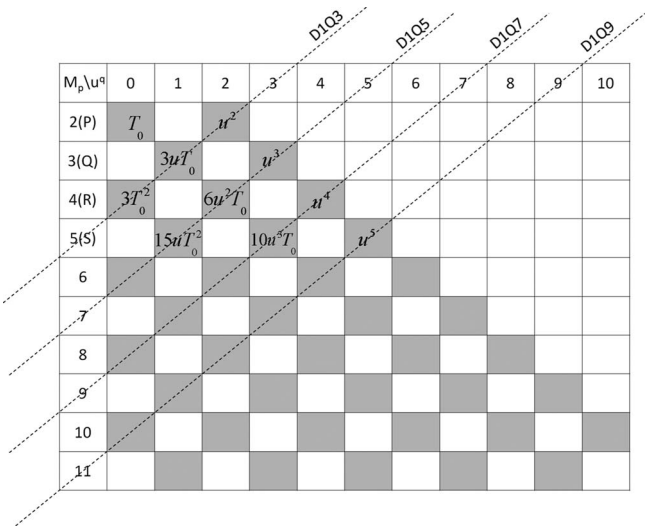

FIG. 5. Convergence of equilibrium moments for various discrete velocity sets. The rows indicate the Maxwell-Boltzmann moments M_p^{MB} of order p, while the columns refer to their expansion into powers of velocity u^q. The nonzero terms of the expansion are indicated with filled boxes. The terms on or above the line are correctly recovered by a particular integer-valued D1Qn_d family.

We have further checked the above-mentioned monotonicity by considering the nine-velocity lattice (see Appendix D). As expected, the order of isotropy becomes $\varphi=12$, i.e., two orders higher compared to the D1Q7 lattice. In Table II, we bring together the orders of isotropy for the shortest D1Q($1+2k$) lattices (odd number of velocities) for $k=1,\ldots,4$.

Considering lattices up to the nine-velocity lattice, it can be conjectured that the monotonicity of the order of isotropy φ holds for all higher-order lattices. The order of isotropy φ, introduced above to characterize the one-dimensional lattices, applies also to their two- and three-dimensional extensions considered in Sec. III. Independent of entropy estimates, similar estimates of isotropy have been recently reported in [19].

TABLE II. The shortest lattices with odd number of velocities, $n_d=1+2q$, $q=1,2,3,4$.

n_d	c_i	φ
3	$\{0,\pm 1\}$	6
5	$\{0,\pm 1,\pm 3\}$	8
7	$\{0,\pm 1,\pm 2,\pm 3\}$	10
9	$\{0,\pm 1,\pm 2,\pm 3,\pm 5\}$	12

C. Instability of lattices

To this end, we have established how to construct lattices, in one dimension, to any desired order of accuracy. We have also pointed out that the entropic construction does not admit all integer-valued lattices. In other words, there is a nontrivial selection of lattices that are *chosen* by the requirement of existence of an entropy function. For example, the shortest five-velocity set that appears in our construction is the ZOT lattice $\{0,\pm1,\pm3\}$, and not the set $\{0,\pm1,\pm2\}$, which could have been obtained by relaxing the entropy requirement and simply enforcing the matching of higher-order equilibrium moments to the MB expressions. We recall that the $\{0,\pm1,\pm2\}$ lattice is ruled out by the entropic construction since the reference temperature (5) becomes complex valued.

We remark that, although a number of ways exist for setting up a lattice Boltzmann scheme on a given lattice, none of the theories so far has attempted to explain the relation between numerical stability and the lattice. A popular way of establishing a LB scheme is by discretizing (followed by truncating) the local Maxwellian on a given lattice to obtain the equilibrium distributions and thus establishing the LBGK scheme. In this process, no assessment of stability or instability of the resulting LB models is possible. A trial and error procedure was the only way of searching for more accurate and stable lattices. Thus the entropic construction explains the stability and also the instability of certain lattices. Loosely defining the notion of stability of a lattice, it can be said that a LBGK simulation, together with its lattice, is stable if its grid requirements are comparable to that of a direct numerical simulation (DNS). Or, alternatively, one could start with the assumption that the D2Q9 lattice is stable, and any lattice that requires much more spatial resolution than the D2Q9 lattice is unstable.

Now, let us consider the two lattices $\{0,\pm1,\pm3\}$ and $\{0,\pm1,\pm2\}$, one supported by the entropy function, the other not. The $\{0,\pm1,\pm2\}$ lattice was considered a number of times in the past (see, for example, [5,13,20]); hence we take the equilibrium distribution for it from the literature [5] and perform a simulation to compare it with the entropic $\{0,\pm1,\pm3\}$ lattice. Once the equilibrium distributions are known, a standard LBGK discretization scheme (3), with relaxation time $\omega=2/(2\tau+1)$, was applied to both the lattices.

A standard test case in one dimension is the shock tube problem [17]. The initial condition for the simulation is a density step $\rho=3.0$ for $x<L/2$ (L is the length of domain), $\rho=1.0$ for $x>L/2$ (as in [5]). Both the models were tested at various values of the kinematic viscosity. The $\{0,\pm1,\pm3\}$ lattice is stable at any value of the viscosity. This is in drastic contrast to the $\{0,\pm1,\pm2\}$ lattice, which is numerically unstable even for moderate ν. A typical situation is shown in Fig. 6, corresponding to $\nu=0.138$. The snapshot of the density profile is taken a few time steps before the run for the $\{0,\pm1,\pm2\}$ lattice terminates; the instability pattern is clearly visible; the density at some lattice nodes becomes negative. The oscillatory pattern of the $\{0,\pm1,\pm3\}$ lattice at the shock is due to lack of artificial diffusivity and is pertinent to all lattice Boltzmann schemes. Thus, the LB

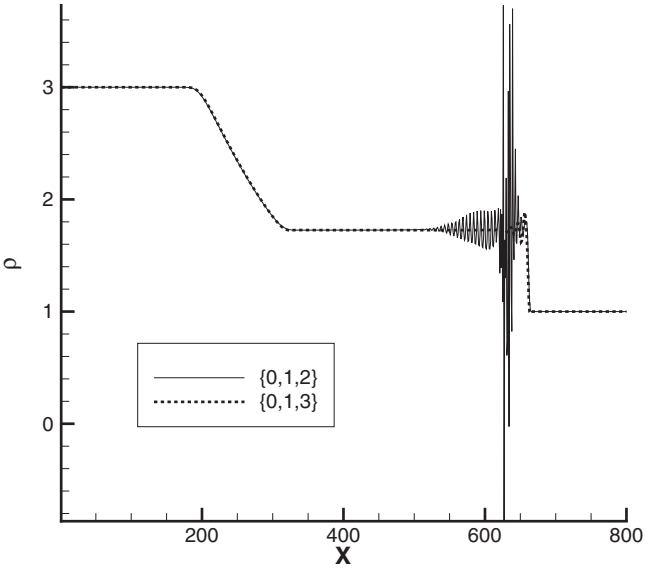

FIG. 6. Simulation of one-dimensional shock tube problem on $\{0,\pm1,\pm3\}$ (present) and $\{0,\pm1,\pm2\}$ lattices.

models based on the entropic considerations are stable, and clearly outperform the nonentropic models.

It must be remembered that both the lattices, the $\{0,\pm1,\pm2\}$ (equilibrium from the literature) and the $\{0,\pm1,\pm3\}$ lattice, fully recover the third-order moment Q^{eq}, and the order of isotropy is the same for both lattices. The choice of weights and reference temperature is different for both lattices, thus enabling the accuracy of the third-order moment to remain the same. However, we see that when a lattice is not supported by entropy it is unstable in simulations.

It is long known that the $\{0,\pm1,\pm2\}$ lattice is numerically unstable. Hence, LB users did not switch to the more accurate and completely Galilean-invariant $\{0,\pm1,\pm2\}$ lattice. The simple $\{0,\pm1\}$ lattice and its higher-dimensional extensions were used instead, in spite of their u^3 deviations and hence their inability to recover the Navier-Stokes equations completely. In some of the earlier studies, the pattern of instability of the $\{0,\pm1,\pm2\}$ lattice, was attributed to the lattice Boltzmann scheme itself [21], or to the advection part of the LB scheme [15,20], or to the collision of the LB scheme [22], or to insufficient isotropy [19]. In contrast, the present entropic construction attributes this instability to the inappropriate choice of the lattice, and not to the LBGK scheme *per se*. However, it remains to be rigorously proven that all lattices that support an entropy function are stable and the rest are bound to be unstable.

In our study we find that all the lattices that support the entropy function (2) are stable. Another interesting example of how entropy-supported lattices produce stable simulations is given in Appendix B, where it is shown that simulations with a non-Gaussian-shaped equilibrium are also stable.

III. HIGHER DIMENSIONS

A. Generating higher-dimensional lattices from a one-dimensional lattice

The general procedure for constructing lattices in one dimension was presented in the previous section. Let us now

extend these lattices into two and three dimensions. Description of a lattice requires the description of the discrete velocities followed by the weights, the reference temperature, and finally the equilibrium distribution.

The discrete velocities in D dimensions are obtained by taking a tensor product of D copies of a one-dimensional lattice. Let us consider a general 1D, n-bit lattice $c_i = \{0, \pm a_1, \pm a_2, \ldots, \pm a_{(n-1)/2}\}$, assuming n is odd. The procedure remains the same for even number of discrete velocities. A Cartesian representation of the discrete velocities in this one-dimensional lattice is made easy by choosing a reference frame with the zero-velocity population at the origin. All the populations can now be denoted by their coordinates (i), where $i \in \{0, \pm a_1, \pm a_2, \ldots, \pm a_{(n-1)/2}\}$.

A D-dimensional extension of this n-velocity lattice contains n^D discrete velocities. Hence, in two dimensions, we need to specify the coordinates of all the n^2 discrete velocities. With the zero-velocity (rest population) chosen as the origin, all the populations can be described by their coordinates (i,j) where $i,j \in \{0, \pm a_1, \pm a_2, \ldots, \pm a_{(n-1)/2}\}$. Similarly, a 3D extension is possible by representing the populations with their coordinates (i,j,k) with $i,j,k \in \{0, \pm a_1, \pm a_2, \ldots, \pm a_{(n-1)/2}\}$.

After the description of the discrete velocities, we proceed with the description of the weights and of the reference temperature for these higher-dimensional lattices. The reference temperature T_0 remains the same as in the one-dimensional case, i.e., the reference temperature appearing in the equilibrium moments is the same for all the directions (x, y, and z). Obviously, the definition of temperature (or speed of sound) cannot be a function of the direction.

The weights in higher dimensions are obtained as algebraic products of the weights derived in the 1D case. Let us describe the weights for the populations according to an *energy-shell representation*. All the populations (i,j,k) $(D=3)$ or (i,j) $(D=2)$ can be collected into shells with the same value of energy ϵ defined as $\epsilon = i^2 + j^2 + k^2$ $(D=3)$ or $\epsilon = i^2 + j^2$ $(D=2)$. The weights $W_{(i,j,k)}$ or $W_{(i,j)}$ for all the velocities (i,j,k) or (i,j) in a particular energy shell are equally distributed. For a given set of discrete velocities $c = \{0, \pm a_1, \pm a_2, \ldots, \pm a_{(n-1)/2}\}$, in one dimension, this means that both the populations (i) and $(-i)$ have the same weight $W_{(i)} = W_{(-i)}$, $\forall\ i \in c$. In two dimensions, $W_{(i,j)} = W_{(\pm i, \pm j)}$, $\forall\ i,j \in c$, and similarly in three dimensions, $W_{(i,j,k)} = W_{(\pm i, \pm j, \pm k)}$, $\forall\ i,j,k \in c$. Hence, it is sufficient to specify the weight of one discrete velocity per energy shell. Assuming that the weights $W_{(i)}$ of a given one-dimensional lattice c are known, the weights for its two- and three-dimensional extensions, $W_{(i,j)}$ and $W_{(i,j,k)}$, are given by

$$W_{(i,j)} = W_{(i)} \times W_{(j)},$$

$$W_{(i,j,k)} = W_{(i)} \times W_{(j)} \times W_{(k)}, \tag{15}$$

for $D=2$ and $D=3$, respectively. The primary advantage of extending the 1D lattices with the procedure just described is that it retains the order of isotropy φ, and hence the accuracy of the corresponding lattices in higher dimensions. Extensions into higher dimensions would all have the same order of accuracy (again, as compared to Maxwell-Boltzmann moment relations) for all the moments of the equilibrium distribution. Hence, the 1D LB hierarchy established in Sec. II is readily extended to two and three dimensions using this procedure. This is in contrast with other suggestions to construct LB lattices (for example, [15,23]), where independent searches have to be performed in each dimension. The entropic construction thus essentially simplifies the problem of searching for higher-dimensional lattices into the one-dimensional problem that was handled in Sec. II. We shall now consider the five-velocity set $\{0, \pm 1, \pm 3\}$ or D1Q5-ZOT lattice, and establish its induced lattices in two and three dimensions.

B. The D1Q5-ZOT lattice

The one-dimensional zero-one-three (D1Q5-ZOT) lattice is the shortest integer-valued discrete velocity set in the family of five-velocity sets [7]. Due its enhanced accuracy and ease of implementation, this lattice has a potential to replace the existing family generated by the three-velocity D1Q3 set, along with its $D=2$ (D2Q9) and $D=3$ (D3Q15, D3Q19, and D3Q27) extensions. Substituting $m=1$ and $n=3$ into the general expression (5), and using the notation $W_1 = W_{\pm 1}$ and $W_3 = W_{\pm 3}$, we get the weights and the reference temperature for the D1Q5-ZOT lattice as

$$W_0 = \frac{4}{45}(4 + \sqrt{10}), \quad W_1 = \frac{3}{80}(8 - \sqrt{10}),$$

$$W_3 = \frac{1}{720}(16 - 5\sqrt{10}),$$

$$T_0 = 1 - \sqrt{\frac{2}{5}}. \tag{16}$$

C. The D2Q25-ZOT lattice

The discrete velocities of its two-dimensional extension are obtained as a tensor product of the two copies of the D1Q5-ZOT sets (see Fig. 7), while the weights are obtained as the algebraic products of the corresponding one-dimensional weights (16). Thus, the two-dimensional counterpart of the D1Q5-ZOT lattice the D2Q25-ZOT lattice, consists of 5^2 velocities, and can be described with ordered pairs (i,j) $\forall\ i,j \in \{-3,-1,0,1,3\}$, centered around the rest population [24]. The weights for the D2Q25-ZOT lattice can be computed, shellwise, from the one-dimensional weights. The weights of all the discrete velocities, (i,j), in a particular energy shell, $\epsilon = i^2 + j^2$, are the same. Hence,

$$W_{(0,0)} = W_0 \times W_0,$$

$$W_{(0,\pm 1)} = W_{(\pm 1,0)} = W_0 \times W_1,$$

$$W_{(0,\pm 3)} = W_{(\pm 3,0)} = W_0 \times W_3,$$

$$W_{(\pm 1,\pm 1)} = W_1 \times W_1,$$

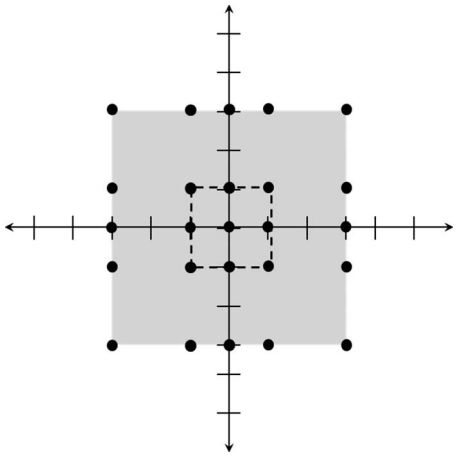

FIG. 7. The D2Q25-ZOT lattice obtained as a tensor product of two five-velocity D1Q5-ZOT lattices.

$$W_{(\pm 1,\pm 3)} = W_{(\pm 3,\pm 1)} = W_1 \times W_3,$$

$$W_{(\pm 3,\pm 3)} = W_3 \times W_3. \tag{17}$$

The reference temperature and hence the speed of sound ($T_0 = c_s^2$) remains the same as in the one-dimensional case (16).

Once the weights are known, the equilibrium populations are derived by minimizing the entropy function H under the constraints of local conservations [25]. In particular, at low Mach numbers, a polynomial approximation to third order in velocity can be written as

$$f_i^{\mathrm{eq}} = \rho W_i \left(1 + \frac{c_{i\alpha} u_\alpha}{T_0} + \frac{u_\alpha u_\beta}{2T_0^2}(c_{i\alpha} c_{i\beta} - T_0 \delta_{\alpha\beta}) + \frac{u_\alpha u_\beta u_\gamma}{6T_0^3} c_{i\gamma}(c_{i\alpha} c_{i\beta} - 3T_0 \delta_{\alpha\beta}) \right) + O(u^4). \tag{18}$$

A faster and a more accurate evaluation of the equilibrium populations at small velocities (which are typically prevalent in LB simulations) is possible with the *product form* introduced in Ref. [25]. In the entropic construction, the equilibrium is defined as a minimum of the H function (2) under the constraints of local conservation laws. If χ, ζ_x, and ζ_y are Lagrange multipliers corresponding to the conservation of mass, the x momentum, and the y momentum respectively, then the equilibrium populations can be written in the product form as

$$f_i^{\mathrm{eq}} = \rho W_i \chi \zeta_x^{c_{ix}} \zeta_y^{c_{iy}}, \tag{19}$$

where the eighth-order accurate expansions of Lagrange multipliers read

$$\chi = \rho \left(1 - \frac{u^2}{2T_0} + \frac{u^4}{8T_0^2} - \frac{(9 - 30T_0 + 18T_0^2)u^6}{144T_0^5} + \chi^{(8)} \right),$$

$$\chi^{(8)} = \frac{1}{384T_0^7}(u^8 - 8\{T_0[T_0(18T_0 - 43) + 22] - 3\}(u_y^2 u_x^6 + u_x^2 u_y^6) - 6\{T_0[T_0(41T_0 - 96) + 47] - 6\}u_y^4 u_x^4),$$

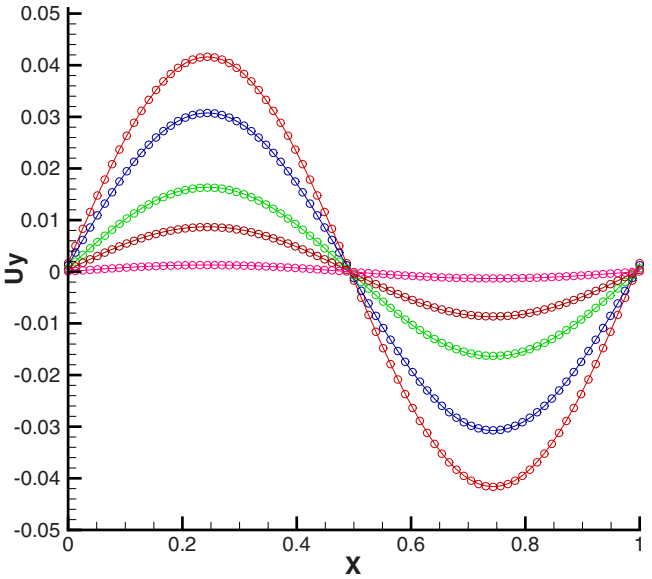

FIG. 8. (Color online) Simulation of Taylor-Green vortex flow with 2D extensions of various four- and five-velocity sets. Line, analytical solution; symbols, simulation.

$$\zeta_\alpha = 1 + \frac{u_\alpha}{T_0} + \frac{u_\alpha^2}{2T_0^2} + \frac{u_\alpha^3}{6T_0^3} + \frac{u_\alpha^4}{24T_0^4} + \frac{[3(T_0 - 2)T_0 + 2]u_\alpha^5}{24T_0^5} + \frac{[18(T_0 - 2)T_0 + 11]u_\alpha^6}{144T_0^6} + \frac{\{3T_0[T_0(11 - 3T_0) - 11] + 8\}u_\alpha^7}{144T_0^7} + \frac{\{24T_0[3(3 - T_0)T_0 - 7] + 35\}u_\alpha^8}{1152T_0^8}. \tag{20}$$

The D2Q25-ZOT lattice, with the above-mentioned equilibrium, recovers the Maxwell-Boltzmann moments with the following accuracy of the moments:

$$P_{\alpha\beta}^{\mathrm{eq}} = \rho T_0 \delta_{\alpha\beta} + \rho u_\alpha u_\beta + O(u^6),$$

$$Q_{\alpha\beta\gamma}^{\mathrm{eq}} = \rho T_0(u_\alpha \delta_{\beta\gamma} + u_\beta \delta_{\alpha\gamma} + u_\gamma \delta_{\alpha\beta}) + \rho u_\alpha u_\beta u_\gamma + O(u^5),$$

$$R_{\alpha\beta}^{\mathrm{eq}} = 4\rho T_0^2 \delta_{\alpha\beta} + \rho T_0 u^2 \delta_{\alpha\beta} + 6\rho T_0 u_\alpha u_\beta + O(u^4). \tag{21}$$

This corresponds to the order of isotropy $\varphi = 8$, the same as in the one-dimensional case. We note that the equilibrium third-order moment $Q_{\alpha\beta\gamma}^{\mathrm{eq}}$ is fully recovered, and, compared to the D2Q9 lattice, the D2Q25-ZOT lattice is two orders more accurate. For isothermal flows, the D2Q25-ZOT lattice accurately recovers the incompressible Navier-Stokes equations (without the u^3 errors). Thus, with the use of the product from, accurate simulations are possible with a minimal computational overhead.

Figure 8 shows the simulation of the 2D Taylor-Green vortex flow. Periodic boundary conditions were imposed in both directions; comparison with the analytical solution (line) is also shown. Moreover, the 2D extensions of all

D1Q5 lattices (and the D1Q4 lattices) listed in Table I were tested for this setup and an equally good agreement was found with the analytical solution.

D. The D3Q125-ZOT lattice

The one-dimensional D1Q5-ZOT lattice manifests itself, via the tensor product, as the $5^3=125$ velocity set in 3D. As already mentioned, the accuracy of the moments for the D3Q125-ZOT velocity lattice is the same as the one-dimensional D1Q5-ZOT lattice, namely,

$$P^{\mathrm{eq}}_{\alpha\beta} = \rho T_0 \delta_{\alpha\beta} + \rho u_\alpha u_\beta + O(u^6),$$

$$Q^{\mathrm{eq}}_{\alpha\beta\gamma} = \rho T_0 (u_\alpha \delta_{\beta\gamma} + u_\beta \delta_{\alpha\gamma} + u_\gamma \delta_{\alpha\beta}) + \rho u_\alpha u_\beta u_\gamma + O(u^5),$$

$$R^{\mathrm{eq}}_{\alpha\beta} = 5\rho T_0^2 \delta_{\alpha\beta} + \rho T_0 u^2 \delta_{\alpha\beta} + 7\rho T_0 u_\alpha u_\beta + O(u^4). \quad (22)$$

The construction of lattices just described extends any one-dimensional lattice of Sec. II into two and three dimensions. All the lattices identified in this way support the entropy function H and demonstrate superior numerical stability. Now it is up to the user to wisely choose the lattice (isotropy) that suits the desired requirements of accuracy. However, the higher-order lattices, although accurate, come with an added computational and storage cost. Although the use of the product form of evaluation of equilibrium reduces the computational cost dramatically, the memory requirement are significantly higher for storing the populations (125 populations per grid point for the D3Q125-ZOT lattice, in particular). Let us now take up the task of reducing the number of discrete velocities in the higher dimensions, considering the D3Q125-ZOT lattice as a particularly important example.

IV. PRUNING OF DISCRETE VELOCITY SETS

It is possible to reduce—or *prune*—the number of discrete velocities, by sacrificing the accuracy of some of the moments, especially the higher-order terms of the higher-order moments. Let us now consider the option of reducing the number of discrete velocities in a given lattice by simply discarding some.

The process of discarding the discrete velocities, or pruning, is made easy when one realizes symmetry conditions. Let us consider discarding a specific discrete velocity (i,j,k) from a given lattice. In order to maintain the x symmetry, or, equivalently, in order to maintain the conservation of x momentum, we need to also discard the discrete velocity $(-i,j,k)$. Similarly, in order to maintain the y and z symmetries (isotropy), we need to discard $(i,-j,k)$ and $(i,j,-k)$. Now, since we have discarded $(i,-j,k)$, we need to further discard its x and z reflections $(-i,-j,k)$ and $(i,-j,-k)$, to maintain x and z symmetries for $(i,-j,k)$. This process continues until we have discarded all the velocities of the form $(\pm i, \pm j, \pm k)$. Equivalently, one could argue that all the populations belonging to a particular energy shell ϵ ($\epsilon = i^2 + j^2 + k^2$) should be retained or discarded as a set.

Hence, let us collate the discrete velocities of the D3Q125-ZOT set, $(i,j,k)\ \forall\ \ i,j,k \in \{-3,-1,0,+1,+3\}$, into energy-shell groups. The totality of the 125 velocities set can be described by ten energy-shell groups from $\epsilon=0$ to 27. The energy shells along with the number of discrete velocities $n_d^{(\epsilon)}$ in each of the shells ϵ are presented in Table III.

TABLE III. Energy-shell representation of the D3Q125-ZOT lattice.

ϵ	c_i	$n_d^{(\epsilon)}$
0	(0,0,0)	1
1	$(\pm1,0,0)$	6
2	$(\pm1,\pm1,0)$	12
3	$(\pm1,\pm1,\pm1)$	8
9	$(\pm3,0,0)$	6
10	$(\pm1,\pm3,0)$	24
11	$(\pm1,\pm1,\pm3)$	24
18	$(\pm3,\pm3,0)$	12
19	$(\pm1,\pm3,\pm3)$	24
27	$(\pm3,\pm3,\pm3)$	8

Certain observations can be made from this representation. For example, the lattice described by the first three energy shells of Table III is the familiar D3Q15 lattice. That is, if we were to heavily prune the D3Q125-ZOT velocity set by discarding all the discrete velocities except the ones belonging to the first three energy shells in Table III, we get back the standard D3Q15 lattice. Similarly, the first two energy shells combined with the fourth energy shell result in the D3Q19 lattice. The combination of the first four energy shells recovers the D3Q27 lattice. Hence, the D3Q125-ZOT lattice can be seen as the mother lattice that contains all the standard LB lattices inside it.

A. The D3Q41-ZOT lattice

The next question that arises is the issue of accuracy of the prunes of any given lattice. It can be argued that the accuracy of a pruned lattice cannot exceed the accuracy of the mother lattice. This also explains the lower accuracy of the standard D3Q15, D3Q19, and D3Q27 lattices (prunes of the D3Q125-ZOT lattice) as compared to the D3Q125-ZOT lattice. Continuing further with the pruning of the D3Q125-ZOT lattice (searching the energy shells for a prune), one can arrive at the minimum number of velocities required to reproduce the moments of the D3Q125-ZOT velocity set (22)

TABLE IV. Energy shells in the pruned D3Q41-ZOT lattice.

ϵ	c_i	$n_d^{(\epsilon)}$
0	(0,0,0)	1
1	$(\pm1,0,0)$	6
2	$(\pm1,\pm1,0)$	12
3	$(\pm1,\pm1,\pm1)$	8
9	$(\pm3,0,0)$	6
27	$(\pm3,\pm3,\pm3)$	8

with the same order of accuracy. In particular, a D3Q41-ZOT lattice is an interesting prune which retains the same order of accuracy of the equilibrium moments as the full D3Q125-ZOT lattice. The energy shells that are retained in the D3Q41-ZOT lattice are given in Table IV, and their corresponding weights and the reference temperature are as follows:

$$W_{(0,0,0)} = \frac{2}{2025}(5045 - 1507\sqrt{10}),$$

$$W_{(1,0,0)} = \frac{37}{5\sqrt{10}} - \frac{91}{40}, \quad W_{(1,1,0)} = \frac{1}{50}(55 - 17\sqrt{10}),$$

$$W_{(1,1,1)} = \frac{233\sqrt{10} - 730}{1600}, \quad W_{(3,0,0)} = \frac{295 - 92\sqrt{10}}{16\,200},$$

$$W_{(3,3,3)} = \frac{130 - 41\sqrt{10}}{129\,600}, \quad T_0 = 1 - \sqrt{\frac{2}{5}}. \tag{23}$$

The 41-velocity lattice is shown in Fig. 9. Once we have identified the energy shells that need to be retained, we can construct the equilibrium by minimizing the H function under the constraints of local conservation laws (entropic construction), thus completing the description of the lattice. We describe here the expressions for the Lagrange multipliers that can be used in the product form ($f_i^{\mathrm{eq}} = \rho W_i \chi \zeta_x^{c_{ix}} \zeta_y^{c_{iy}} \zeta_z^{c_{iz}}$) for evaluation of the equilibrium [these expressions can be significantly simplified, for computational efficiency, upon substituting the value of T_0 from Eq. (23)]:

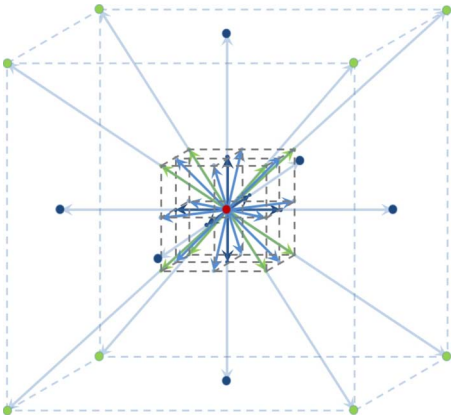

FIG. 9. (Color online) The D3Q41-ZOT lattice. It can described as a D3Q15 lattice stretched by a factor of 3 (shown with lower transparency) and superimposed on a regular D3Q27 lattice (shown brightly) without duplicating the rest population.

$$\chi = 1 - \frac{u^2}{2T_0} + \frac{u^4}{8T_0^2} - \frac{[3 - 2T_0(5 - 3T_0)]u^6}{48T_0^5} + \frac{[5(T_0 - 2)T_0 + 3](u_x^2 + u_y^2)(u_x^2 + u_z^2)(u_y^2 + u_z^2)}{16T_0^5}$$
$$- \frac{\{6 - T_0[6T_0(7T_0 - 16) + 47]\}u^8}{384T_0^7} - \frac{\{T_0[T_0(18T_0 - 43) + 22] - 3\}(u_x^2 + u_y^2)(u_x^2 + u_z^2)(u_y^2 + u_z^2)u^2}{48T_0^7}$$
$$+ \frac{[7T_0(T_0 + 1) - 3](u_x^4 u_y^4 + u_y^4 u_z^4 + u_x^4 u_z^4)}{96T_0^7} + \frac{\{2[14T_0(5T_0 - 1) - 3]\}u_x^2 u_y^2 u_z^2 u^2}{96T_0^7},$$

$$\zeta_x = \frac{u_x}{T_0} + \frac{u_x^2}{2T_0^2} + \frac{u_x^3}{6T_0^3} + \frac{u_x^4}{24T_0^4} + \frac{[3(T_0 - 2)T_0 + 2]u_x^5}{24T_0^5} + \frac{[18(T_0 - 2)T_0 + 11]u_x^6}{144T_0^6} + \frac{\{8 - 3T_0[T_0(3T_0 - 11) + 11]\}u_x^7}{144T_0^7}$$
$$+ \frac{\{35 - 24T_0[3(T_0 - 3)T_0 + 7]\}u_x^8}{1152T_0^8} + \frac{(3T_0 - 1)u_x}{48T_0^6}\left(1 + \frac{u_x}{T_0}\right)\{[(T_0 - 3)u_y^4 + (T_0 - 9)u_z^2 u_y^2 + (T_0 - 3)u_z^4]u_x^2$$
$$+ (T_0 - 9)u_y^2 u_z^2 u^2\},$$

$$\zeta_y = \frac{u_y}{T_0} + \frac{u_y^2}{2T_0^2} + \frac{u_y^3}{6T_0^3} + \frac{u_y^4}{24T_0^4} + \frac{[3(T_0 - 2)T_0 + 2]u_y^5}{24T_0^5} + \frac{[18(T_0 - 2)T_0 + 11]u_y^6}{144T_0^6} + \frac{\{8 - 3T_0[T_0(3T_0 - 11) + 11]\}u_y^7}{144T_0^7}$$
$$+ \frac{\{35 - 24T_0[3(T_0 - 3)T_0 + 7]\}u_y^8}{1152T_0^8} + \frac{(3T_0 - 1)u_y}{48T_0^6}\left(1 + \frac{u_y}{T_0}\right)\{[(T_0 - 3)u_x^4 + (T_0 - 9)u_z^2 u_x^2 + (T_0 - 3)u_z^4]u_y^2$$
$$+ (T_0 - 9)u_x^2 u_z^2 u^2\},$$

$$\zeta_z = \frac{u_z}{T_0} + \frac{u_z^2}{2T_0^2} + \frac{u_z^3}{6T_0^3} + \frac{u_z^4}{24T_0^4} + \frac{[3(T_0-2)T_0+2]u_z^5}{24T_0^5} + \frac{[18(T_0-2)T_0+11]u_z^6}{144T_0^6} + \frac{\{8-3T_0[T_0(3T_0-11)+11]\}u_z^7}{144T_0^7} + \frac{\{35-24T_0[3(T_0-3)T_0+7]\}u_z^8}{1152T_0^8} + \frac{(3T_0-1)u_z}{48T_0^6}\left(1+\frac{u_z}{T_0}\right) \times \{[(T_0-3)u_x^4 + (T_0-9)u_y^2u_x^2 + (T_0-3)u_y^4]u_z^2 + (T_0-9)u_x^2u_y^2u^2\}. \quad (24)$$

Existence of the D3Q41-ZOT velocity set (as a prune of the D3Q125-ZOT lattice) is not surprising. Indeed, it is similar to the D3Q15 and the D3Q19 lattices which can be regarded as the prunes of the D3Q27 lattice. In the latter case, the order of accuracy of the moments of D3Q15 and of D3Q19 LB lattices remains the same as that of the D3Q27 lattice but the number of discrete velocities is significantly reduced from 27 to 15 (or 19). The 15-, 19-, and 27-velocity sets all have errors of order u^4 in the equilibrium pressure tensor $P^{\mathrm{eq}}_{\alpha\beta}$, order u^3 in the third-order moments $Q^{\mathrm{eq}}_{\alpha\beta\gamma}$, and so on. Although the number of error terms in the 15-velocity lattice is higher than those in the 27-velocity case, it can be argued that these errors are of the same order and hence do not show up in the simulations [similar to the (41–125)-velocity cases]. The 41-velocity set is hence two orders more accurate than the 15-, 19-, or 27- (D1Q3 family) velocity sets and, thanks to the product form, it is only 2.3 times slower compared to the 15-velocity set.

V. NUMERICAL EXAMPLE

We present here a resolved direct numerical simulation using the D3Q41-ZOT lattice from Sec. IV A. A well-known 3D setup of Taylor-Green vortex flow is simulated using the 41-velocity lattice and compared to the results obtained from DNS using the higher-order spectral element method [26]. The grid sizes (64^3–128^3) were chosen to approximately match the total number of degrees of freedom (number of elements times number of collocation points raised to 3) used in the spectral element simulation [26]. The equilibrium distributions were evaluated using the product form, $f_i^{\mathrm{eq}} = \rho W_i \chi \zeta_x^{c_{ix}} \zeta_y^{c_{iy}} \zeta_z^{c_{iz}}$, with χ, ζ_x, ζ_y, ζ_z given by Eq. (24). As the flow evolves from its highly symmetric initial conditions, the enstrophy of the system (given by $\Omega = 0.5\int w^2 dx\, dy\, dz$, where $w = \nabla \times u$ is the vorticity) grows until a certain time and then decays as the viscous forces take over the vortex stretching process. Good agreement was found between the 41-velocity LB simulations and the spectral element simulations (see Fig. 10) at various Reynolds numbers. Further high-resolution simulations at higher Reynolds numbers will be presented in a separate communication.

VI. DISCUSSION

In this paper, we have shown that, in order to establish a working higher-order lattice Boltzmann scheme, it is crucial to choose the right set of discrete velocities along with their weights and a reference temperature. A hierarchy of LB lattices with a systematic increase in accuracy was presented, in all three dimensions. The theory presented herein is completely general, and accounts for *all* possible Cartesian lattices suitable for developing the LB models. The simple lattices used in LB simulations (the D1Q3 lattice and its two- and three-dimensional extensions) follow as low-order approximations in this construction. Other LB lattices obtained from Gauss-Hermite quadrature are derived from the present construction, as limiting cases of integer-valued lattices, without any quadrature assumptions. Most importantly, integer-valued lattices which preserve the essence and primary advantage of lattice Boltzmann methods, are identified to any desired order of accuracy.

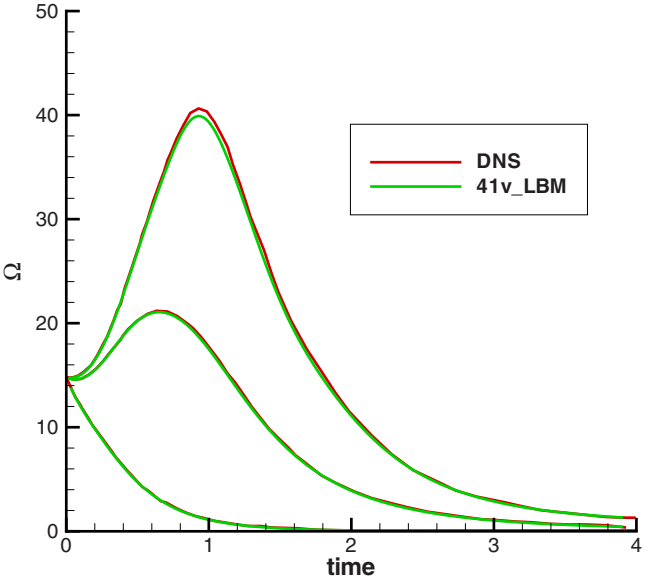

FIG. 10. (Color online) Enstrophy history in the Taylor-Green vortex flow at Re=100,500,1000.

Apart from constructing stable lattices, an insight is provided as to why some of the lattices (already present in the LB literature) are unstable. Until now, the instability of some lattices was interpreted as inability of the LB scheme, or luck, or inconsistency of LB advection or collision [15,20,22]. In the above construction, an infinite number of stable lattices are identified. It is impossible to simulate all the lattices identified herein. Many lattices including prunes were tested for stability and without exception, all the lattices that supported an entropy function were found to be stable [27]. Applications of these lattices to other flow situations like multiphase flows, multicomponent flows, microflows, etc. can lead to interesting results; for example, certain lattices might be preferable for certain applications, etc.

In higher dimensions, the newly introduced concept of pruning also promises to systematically search for the lattices which best suit an application. Also, pruning can help in significantly reducing the number of discrete velocities, in higher dimensions. The process of pruning should be preferred over adding of energy shells or discrete velocities, because pruning can avoid pitfalls like the $\{0, \pm 1, \pm 2\}$ lattice. By taking a $\{0, \pm 1\}$ lattice and adding energy shells,

nothing can be said about the stability of newly obtained lattices. Also, adding is an infinite and uncontrolled process, in terms of errors; while pruning is a finite process and we always know the upper and lower bounds of the accuracy. All the lattices that can identified by adding energy shells can be identified in a more systematic way by pruning.

Finally, it must be noted that, for large discrete velocity sets, the computational costs can be reduced by one to two orders of magnitude by switching from the series evaluation of equilibrium to the product form of evaluation of equilibrium [25].

APPENDIX A: ACCURACY OF D2Q9 LATTICE

It is useful to reconsider the popular one-dimensional three-velocity lattice $\{0, \pm 1\}$, and its extensions in two and three dimensions—the D2Q9 and D3Q27 velocity lattices. The other two popular three-dimensional lattices used in the LB method—the D3Q15 and D3Q19 velocity lattices—are prunes of the D3Q27 velocity set and hence are less accurate. It must be remembered that, to date, a majority of LB simulations are performed using this family of the three-velocity set (D1Q3). Let us enumerate the accuracy of the moments (of equilibrium) using the example of the D2Q9 velocity lattice. To start off, we need the equilibrium distribution to a good order of accuracy. Often in the literature a quadratic approximation to the equilibrium distribution,

$$f_i^{\mathrm{eq}}(\rho,\mathbf{j}) = W_i\left(\rho + \frac{j_\alpha c_{i\alpha}}{c_{\mathrm{s}}^2} + \frac{1}{2c_{\mathrm{s}}^4} j_\alpha j_\beta (c_{i\alpha}c_{i\beta} - c_{\mathrm{s}}^2\delta_{\alpha\beta})\right) + O(u^3), \tag{A1}$$

is used. But unfortunately this expression assumes a cubic error (u^3) in the equilibrium and hence in all its subsequent moments. Let us consider here the fourth-order equilibrium distribution obtained by expanding the Maxwell-Boltzmann distribution on nodes of the third-order Gauss-Hermite quadrature, i.e., expanding the MB distributions on a lattice defined by the roots of the third-order Hermite polynomial. It must be noted that such an expansion must be truncated at a certain order (in this case, max u^5) in order to avoid errors in the conservation laws. The moments of the D2Q9 velocity lattice, accurate to order u^4, read

$$P_{xx}^{\mathrm{eq}} = \frac{\rho}{3} + \rho u_x^2 - \underline{\frac{3\rho u_x^4}{4}}, \quad P_{xy}^{\mathrm{eq}} = \rho u_x u_y,$$

$$P_{yy}^{\mathrm{eq}} = \frac{\rho}{3} + \rho u_y^2 - \underline{\frac{3\rho u_y^4}{4}},$$

$$Q_{xxx}^{\mathrm{eq}} = \rho u_x + \underline{0 \times \rho u^3}, \quad Q_{xxy}^{\mathrm{eq}} = \frac{\rho u_y}{3} + \rho u_y u_x^2,$$

$$Q_{xyy}^{\mathrm{eq}} = \frac{\rho u_x}{3} + \rho u_x u_y^2, \quad Q_{yyy}^{\mathrm{eq}} = \rho u_y + \underline{0 \times \rho u^3},$$

$$R_{xxxx}^{\mathrm{eq}} = \frac{\rho}{3} + \underline{\rho u_x^2 - \frac{3\rho u_x^4}{4}},$$

$$R_{xxyy}^{\mathrm{eq}} = \frac{\rho}{9} + \frac{1}{3}\rho u^2 + \rho u_x^2 u_y^2 - \underline{\frac{1}{4}\rho(u_x^4 + u_y^4)}. \tag{A2}$$

The errors, i.e., the deviation from the moments of the Maxwell-Boltzmann distributions, are underlined. In order to avoid seeing these errors in a simulation, the magnitude of velocity u is restricted to $u < 10^{-2}$ in LB simulations. For simple isothermal fluid flows these errors are not significant; and this lattice was shown to accurately capture the behavior of incompressible Navier-Stokes equations in many different flow setups [1].

APPENDIX B: NON-GAUSSIAN EQUILIBRIA

The entropic construction proceeds without assuming the Gauss-Hermite or any other quadrature. Inputs to the construction are the requirements of the H function, and of the MB form for the higher-order equilibrium moments. Remarkably, this procedure recovered the Gauss-Hermite discretization at its limiting cases. The procedure has led also to the discovery of lattices that cannot be represented by the Gauss-Hermite quadrature; for example, the integer-valued higher-order lattices. The shape of the equilibrium distribution for all the lattices reported here and elsewhere in the LB literature resembles a Gaussian distribution. That is, the weights W_i are maximal for rest populations (corresponding to $c_i = 0$) and are rapidly decaying with the velocity magnitude. We term this behavior Gaussian-like.

Interestingly, the integer-valued discrete velocities with a Gaussian-like shape of the equilibrium are not the only solutions recovered by the entropic construction. For the lattices with more than three discrete velocities ($D=1$, $n_d > 3$) it was possible to find an alternative combination of W_i and T_0 which lead to non-Gaussian equilibria.

Let us illustrate this with the example of the five-velocity set $\{0, \pm n, \pm m\}$. One set of the weights and of the reference temperatures was found above [see Eq. (5)]. A different sets of weights and reference temperatures for the same lattices was found as (notice the difference in the sign in front of the square root)

$$W_0 = \frac{-3m^4 - 3n^4 + 54m^2n^2 - (m^2+n^2)\sqrt{9m^4 - 42n^2m^2 + 9n^4}}{75m^2n^2},$$

$$W_{\pm m} = \frac{9m^4 - 6n^4 - 27n^2m^2 + (3m^2 - 2n^2)\sqrt{9m^4 - 42n^2m^2 + 9n^4}}{300m^2(m^2 - n^2)},$$

$$W_{\pm n} = \frac{9n^4 - 6m^4 - 27n^2m^2 + (3n^2 - 2m^2)\sqrt{9m^4 - 42n^2m^2 + 9n^4}}{300n^2(n^2 - m^2)},$$

$$T_0 = \frac{3m^2 + 3n^2 + \sqrt{9m^4 - 42n^2m^2 + 9n^4}}{30}. \tag{B1}$$

Noting that, for (5) the reference temperature is always less than unity, and for (B1) it is always greater than unity; we refer to the two solutions as the "lower-T_0" ($T_0 \leqslant 1$) and "higher-T_0" ($T_0 \geqslant 1$) cases. Both sets of the weights and reference temperatures recover the equilibrium third-order moment, $Q^{\mathrm{eq}} = \Sigma_{i=1}^{n_d} f_i \mathrm{eq} c_i^3$, correctly up to order u^3, and hence are both valid candidates for the LB construction. However, they recover the equilibrium fourth- (R^{eq}) and the higher-order moments with a different accuracy. In other words, although the order of isotropy $\varphi = 8$ is the same for both the solutions, the numerical coefficients with which the errors appear in the higher-order terms are different. We have earlier reported that the choice of m and n affect the accuracy of the moments, and a good choice of m and n, or equivalently $m/n = r_5$, can push the error to one order higher in the moment chain. In this particular case, the choice of $r_5 = r_5^* = (\sqrt{5} - \sqrt{2})/\sqrt{3}$ improves the u^4 term in the fourth-order moment. This ratio of the discrete velocities r_5^* is the ratio of the nontrivial roots of the fifth-order Hermite polynomial. At $r_5 = r_5^*$ we recover the fifth-order Gauss-Hermite quadrature from the entropic construction.

Interestingly, the limit of the Gauss-Hermite quadrature (where $r_5 = r_5^*$, $T_0^* = 1$) is reached with both the lower- and higher-T_0 cases. That is, both sets (5) and (B1) converge to the same limit of the Gauss-Hermite quadrature as $r_5 \to r_5^*$. Moreover, the higher-T_0 case results in non-Gaussian weights before it reaches the limit. This is illustrated in Figs. 11 and 12. Figure 11 corresponds to $r_5 = 0.35$ (away from the limit r_5^*) while Fig. 12 corresponds to $r_5 = 0.4740$ (close to the limiting value $r_5^* \approx 0.474\,49$). The lattice with $r_5 = 0.35$ clearly shows a non-Gaussian shape for the equilibrium distribution in the higher-T_0 case (B1).

To the best of our knowledge, this is the first time the explicitly non-Gaussian distribution of the equilibrium weights has appeared in the LB context. Simulations with the non-Gaussian weights (B1) revealed no difference in numerical stability which can be attributed to the fact that both lower- and higher-T_0 LB models are supported by the entropy function. In this paper, we consider only the lower reference temperature case (5) where the equilibrium is Gaussian-like.

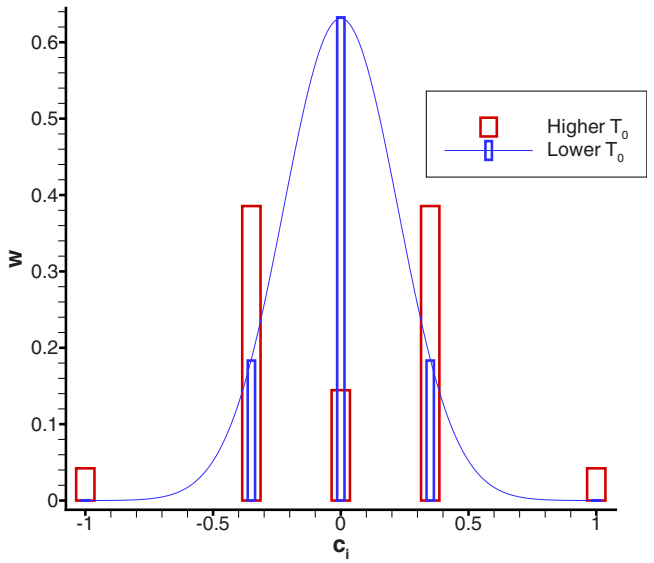

FIG. 11. (Color online) Equilibrium distribution, at zero velocity, for the lattice $c_i = \{0, \pm 0.35, \pm 1\}$, for both possible reference temperatures. A curve with the shape $\exp(-ax^2)$ is fitted onto the weights for the lower-T_0 case to guide the eye [it should not be confused with the curve $\exp(-x^2/2T_0)$].

APPENDIX C: 1D SEVEN VELOCITY SET

For a general seven-velocity set $\{0, \pm 1, \pm m, \pm n\}$, the expressions for the weights and the reference temperature are

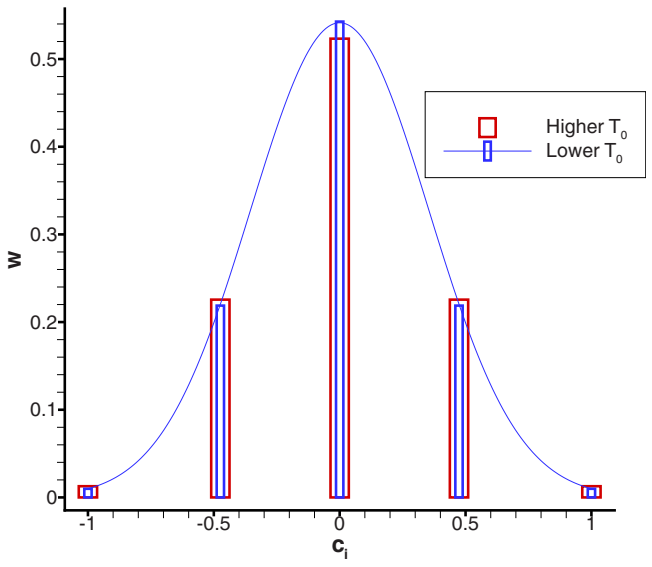

FIG. 12. (Color online) Equilibrium distribution, at zero velocity, for the lattice $c_i = \{0, \pm 0.4740, \pm 1\}$, for both possible reference temperatures.

$$W_0 = \frac{-15T_0^3 + 3(m^2+n^2+1)T_0^2 - [(n^2+1)m^2+n^2]T_0 + m^2n^2}{m^2n^2},$$

$$W_{\pm 1} = \{2(m^2-1)[(T_0-1)m^2 - 3T_0^2 + T_0]\}^{-1}\Bigg((T_0[m^2n^2 + 3T_0^2 - (m^2+n^2)T_0][m^2 + 15T_0^2 - 3(m^2+1)T_0]\{-15T_0^3 + 3(m^2+n^2 + 1)T_0^2 - [(n^2+1)m^2+n^2]T_0 + m^2n^2\})(n^2(n^2-1)\{[(T_0-1)n^2 - 3T_0^2 + T_0]m^2 + T_0[n^2 + 15T_0^2 - 3(n^2+1)T_0]\})^{-1} - \frac{(m^2-3T_0)T_0\{-15T_0^3 + 3(m^2+n^2+1)T_0^2 - [(n^2+1)m^2+n^2]T_0 + m^2n^2\}}{n^2}\Bigg),$$

$$W_{\pm n} = (T_0[m^2 + 15T_0^2 - 3(m^2+1)T_0]\{-15T_0^3 + 3(m^2+n^2+1)T_0^2 - [(n^2+1)m^2+n^2]T_0 + m^2n^2\}) \times (2(m-n)n^2(m+n)(n^2-1)\{[(T_0-1)n^2 - 3T_0^2 + T_0]m^2 + T_0[n^2 + 15T_0^2 - 3(n^2+1)T_0]\})^{-1},$$

$$W_{\pm m} = -\Bigg(\frac{T_0(3T_0-1)\{-15T_0^3 + 3(m^2+n^2+1)T_0^2 - [(n^2+1)m^2+n^2]T_0 + m^2n^2\}}{m^2n^2} + (T_0((T_0-1)n^2 - 3T_0^2 + T_0)[m^2 + 15T_0^2 - 3(m^2+1)T_0]\{-15T_0^3 + 3(m^2+n^2+1)T_0^2 - [(n^2+1)m^2+n^2]T_0 + m^2n^2\}) \times ((m-n)n^2(m+n)\{[(T_0-1)n^2 - 3T_0^2 + T_0]m^2 + T_0[n^2 + 15T_0^2 - 3(n^2+1)T_0]\})\Bigg) \times \{2(m^2-1)[(T_0-1)m^2 - 3T_0^2 + T_0]\}^{-1},$$

$$T_0 = \frac{1}{210}\Bigg(10(m^2+n^2+1) - 2^{2/3}\Bigg[-250m^6 + 825(n^2+1)m^4 + 75(11n^4 - 104n^2 + 11)m^2 - 25(n^2+1)(10n^4 - 43n^2 + 10) + \frac{1}{27}(4\{945[(n^2+1)m^2+n^2] - 225(m^2+n^2+1)^2\}^3 + 455\,625[10m^6 - 33(n^2+1)m^4 + (-33n^4 + 312n^2 - 33)m^2 + (n^2+1)(10n^4 - 43n^2 + 10)]^2)^{1/2}\Bigg]^{1/3} - 2\sqrt[3]{25}^{2/3}[5m^4 - 11(n^2+1)m^2 + 5n^4 - 11n^2 + 5]\Bigg[-50m^6 + 165(n^2+1)m^4 + 15(11n^4 - 104n^2 + 11)m^2 - 5(n^2+1)(10n^4 - 43n^2 + 10) + \frac{1}{135}(4\{945[(n^2+1)m^2+n^2] - 225(m^2+n^2+1)^2\}^3 + 455\,625[10m^6 - 33(n^2+1)m^4 + (-33n^4 + 312n^2 - 33)m^2 + (n^2+1)(10n^4 - 43n^2 + 10)]^2)\Bigg]^{-1/3}\Bigg). \quad \text{(C1)}$$

In order to compute the equilibrium, using the product form of the evaluation of equilibrium $f_i^{\mathrm{eq}} = \rho W_i \chi \zeta_x^{c_{ix}}$, we present below the Lagrange multipliers. If needed, these expressions can be substituted in the product form and expanded further (followed by truncation) to obtain conventional series expressions for the equilibrium. The Lagrange multipliers for this general case are

$$\chi = 1 - \frac{u_x^2}{2T_0} + \frac{u_x^4}{8T_0^2} - \frac{u_x^6}{48T_0^3} - \frac{\{[(3T_0-1)n^2 + 3(1-5T_0)T_0]m^2 + 3T_0[n^2 + 10T_0^2 - 5(n^2+1)T_0] + 60\}u_x^8}{5760T_0^7},$$

$$\zeta_x = 1 + \frac{u_x}{T_0} + \frac{u_x^2}{2T_0^2} + \frac{u_x^3}{6T_0^3} + \frac{u_x^4}{24T_0^4} + \frac{u_x^5}{120T_0^5} + \frac{u_x^6}{720T_0^6} + \zeta_x^{(7)} + \zeta_x^{(8)},$$

$$\zeta_x^{(7)} = \frac{\{[(3T_0-1)n^2 + 3(1-5T_0)T_0]m^2 + 3T_0[n^2 - 5(n^2+1)T_0] + 106\}u_x^7}{5040T_0^7},$$

$$\zeta_x^{(8)} = \frac{\{8[(3T_0-1)n^2 + 3(1-5T_0)T_0]m^2 + 24T_0[n^2 - 5(n^2+1)T_0] + 841\}u_x^8}{40\,320T_0^8}. \quad \text{(C2)}$$

The free parameters in the seven-velocity sets (C1) can be used to tune the accuracy of the higher-order moments in this family. Let us, however, report here the integer-valued lattice with shortest links. For the seven-velocity family this lattice in 1D is the $\{0, \pm 1, \pm 2, \pm 3\}$ lattice. For this lattice the weights, the reference temperature, and the Lagrange multipliers are given by

$$W_0 = \frac{1}{36}\{T_0[3(14-5T_0)T_0-49]+36\},$$

$$W_{\pm 1} = \frac{1}{16}T_0[T_0(5T_0-13)+12],$$

$$W_{\pm 2} = \frac{1}{40}T_0[5(2-T_0)T_0-3],$$

$$W_{\pm 3} = \frac{1}{720}T_0[15(T_0-1)T_0+4],$$

$$T_0 = \frac{2}{3}+\frac{1}{3}\sqrt[3]{\frac{7}{5(-5+3\sqrt{30})}}-\frac{\sqrt[3]{\frac{1}{7}(-5+3\sqrt{30})}}{35^{2/3}} \approx 0.697\,953\,322\,019\,683\,1, \quad \text{(C3)}$$

$$\chi = 1-\frac{u_x^2}{2T_0}+\frac{u_x^4}{8T_0^2}-\frac{u_x^6}{48T_0^3}+\frac{\{8-T_0[10(T_0-7)T_0+49]\}u_x^8}{1920T_0^7}, \quad \text{(C4)}$$

$$\zeta_x = 1+\frac{u_x}{T_0}+\frac{u_x^2}{2T_0^2}+\frac{u_x^3}{6T_0^3}+\frac{u_x^4}{24T_0^4}+\frac{u_x^5}{120T_0^5}+\frac{u_x^6}{720T_0^6}+\zeta_x^{(7)}+\zeta_x^{(8)},$$

$$\zeta_x^{(7)} = -\frac{[3T_0(10T_0-7)-10]u_x^7}{720T_0^7},$$

$$\zeta_x^{(8)} = -\frac{[24T_0(10T_0-7)-79]u_x^8}{5760T_0^8}. \quad \text{(C5)}$$

The accuracy of the $\{0, \pm 1, \pm 2, \pm 3\}$ lattice is given by Eq. (10).

APPENDIX D: 1D NINE-VELOCITY SET

Although it is possible to consider a general nine-velocity lattice $\{0, \pm m, \pm n, \pm q, \pm p\}$, generic expressions for weights in terms of n, m, p are bulky, and we present here the result assuming $m=1$, $n=2$, $q=3$. The weights and reference temperature in this case read

$$W_0 = \frac{\{T_0[3(14-5T_0)T_0-49]+36\}p^2+3T_0\{7T_0[5(T_0-2)T_0+7]-12\}}{36p^2},$$

$$W_{\pm 1} = \frac{T_0\{[T_0(5T_0-13)+12]p^2+T_0[5(13-7T_0)T_0-36]\}}{16(p^2-1)},$$

$$W_{\pm 2} = \frac{T_0\{[-5(T_0-2)T_0-3]p^2+T_0[5T_0(7T_0-10)+9]\}}{40(p^2-4)},$$

$$W_{\pm 3} = \frac{T_0\{p^2[15(T_0-1)T_0+4]-3T_0[5T_0(7T_0-5)+4]\}}{720(p^2-9)}, \quad W_{\pm p} = \frac{3T_0\{7T_0[5(T_0-2)T_0+7]-12\}}{2p^2[p^2(p^2-7)^2-36]}, \quad \text{(D1)}$$

$$T_0 = \frac{p^2}{36}+\frac{7}{18}-\frac{1}{36\sqrt{35}}\{35(p^2+14)^2-840(2p^2+7)+12\sqrt[3]{35}D_1+[1235^{2/3}(-7p^4+110p^2+203)]D_1\}^{1/2}$$
$$+\frac{1}{18\sqrt{70}}\left(35(p^2+14)^2-840(2p^2+7)-6\sqrt[3]{35}D_1+\frac{635^{2/3}(7p^4-110p^2-203)}{D_1}\right.$$
$$\left.+\frac{\sqrt{35}(-35p^6+1050p^4-8232p^2+4112)}{\sqrt{35(p^2+14)^2-840(2p^2+7)+12\sqrt[3]{35}D_1+D_1^{-1}[1235^{2/3}(-7p^4+110p^2+203)]}}\right)^{1/2},$$

$$D_1 = \sqrt[3]{35p^6-231p^4-7203p^2-3\sqrt{6}\sqrt{D_2}+21979},$$

$$D_2 = 245p^{12}-10780p^{10}+13\,7004p^8-164\,696p^6-3\,442\,481p^4-14\,677\,656p^2+3\,523\,824. \quad \text{(D2)}$$

The numerical values for the reference temperature for a few values of p are

$$T_0|_{p=4} = \text{complex valued},$$

$$T_0|_{p=5} = 0.756\,080\,852\,594\,268\,58,$$

$$T_0|_{p=6} = 0.732\,023\,042\,334\,901\,70,$$

$$T_0|_{p=7} = 0.721\,161\,034\,124\,337\,75,$$

$$T_0|_{p=8} = 0.714\,986\,240\,769\,250\,02. \tag{D3}$$

This is similar to the situation in the five-velocity case where the reference temperature for the $\{0, \pm 1, \pm 2\}$ lattice was complex valued and the first lattice available was the $\{0, \pm 1, \pm 3\}$ lattice. The $\{0, \pm 1, \pm 2\}$ lattice is now considered, through trial and error attempts, as an *unstable* lattice and the $\{0, \pm 1, \pm 3\}$ is gaining momentum in the LB literature. However, the theory of entropic construction could predict the unstable nature of the $\{0, \pm 1, \pm 2\}$ lattice due to its complex-valued reference temperature (during the entropic construction) [7]. Hence based on this construction, the $\{0, \pm 1, \pm 2, \pm 3, \pm 4\}$ lattice can also be predicted to be unstable.

The definition of the lattice is complete once the expressions for equilibrium distribution, or equivalently the expressions for Lagrange multipliers are defined. The expressions for mass and momentum conservation Lagrange multipliers are

$$\chi = 1 - \frac{u_x^2}{2T_0} + \frac{u_x^4}{8T_0^2} - \frac{u_x^6}{48T_0^3} + \frac{u_x^8}{384T_0^4},$$

$$\zeta_x = 1 + \frac{u_x}{T_0} + \frac{u_x^2}{2T_0^2} + \frac{u_x^3}{6T_0^3} + \frac{u_x^4}{24T_0^4} + \frac{u_x^5}{120T_0^5} + \frac{u_x^6}{720T_0^6} + \frac{u_x^7}{5040T_0^7} + \frac{u_x^8}{40\,320T_0^8}. \tag{D4}$$

For completeness, the weights and reference temperature for the shortest integer-valued nine-velocity set $\{0, \pm 1, \pm 2, \pm 3, \pm 5\}$ are listed here:

$$W_0 = \frac{1}{900}(T_0\{3T_0[5T_0(7T_0 - 39) + 399] - 1261\} + 900),$$

$$W_{\pm 1} = -\frac{1}{384}T_0\{T_0[5T_0(7T_0 - 38) + 361] - 300\},$$

$$W_{\pm 2} = \frac{1}{840}T_0\{7T_0[5(T_0 - 5)T_0 + 37] - 75\},$$

$$W_{\pm 3} = -\frac{T_0\{3T_0[5T_0(7T_0 - 30) + 129] - 100\}}{11520},$$

$$W_{\pm 5} = \frac{T_0\{7T_0[5(T_0 - 2)T_0 + 7] - 12\}}{134\,400},$$

$$T_0 = 0.756\,080\,852\,594\,268\,58. \tag{D5}$$

The expressions for Lagrange multipliers for the $\{0, \pm 1, \pm 2, \pm 3, \pm 5\}$ lattice are the same as in the general case of $\{0, \pm 1, \pm 2, \pm 3, \pm p\}$. The accuracy of the equilibrium moments for the $\{0, \pm 1, \pm 2, \pm 3, \pm p\}$ family of lattices is

$$P^{\text{eq}} = \rho T_0 + \rho u^2 + O(u^{10}),$$

$$Q^{\text{eq}} = 3\rho T_0 u + \rho u^3 + O(u^9),$$

$$R^{\text{eq}} = 3\rho T_0^2 + 6\rho T_0 u^2 + \rho u^4 + O(u^8),$$

$$S^{\text{eq}} = 15\rho T_0^2 u + 10\rho T_0 u^3 + \rho u^5 + O(u^7), \tag{D6}$$

where the fifth-order equilibrium moment $S^{\text{eq}} = \Sigma_{i=1}^{n_d} f_i^{\text{eq}} c_i^5$ differs from its Maxwell-Boltzmann form by the terms of order $O(u^7)$.

[1] S. Succi, *The Lattice Boltzmann Equation for Fluid Dynamics and Beyond* (Oxford University Press, Oxford, 2001).

[2] I. V. Karlin, A. Ferrante, and H. C. Öttinger, Europhys. Lett. **47**, 182 (1999).

[3] Y.-H. Qian, D. d'Humieres, and P. Lallemand, Europhys. Lett. **17**, 479 (1992).

[4] S. Ansumali and I. V. Karlin, Phys. Rev. Lett. **95**, 260605 (2005).

[5] Y.-H. Qian and Y. Zhou, Europhys. Lett. **42**, 359 (1998).

[6] X. W. Shan and X. He, Phys. Rev. Lett. **80**, 65 (1998).

[7] S. S. Chikatamarla and I. V. Karlin, Phys. Rev. Lett. **97**, 190601 (2006).

[8] N. I. Prasianakis and I. V. Karlin, Phys. Rev. E **76**, 016702 (2007).

[9] M. R. Swift, E. Orlandini, W. R. Osborn, and J. M. Yeomans, Phys. Rev. E **54**, 5041 (1996).

[10] S. Arcidiacono, I. V. Karlin, J. Mantzaras, and C. E. Frouzakis, Phys. Rev. E **76**, 046703 (2007).

[11] S. Ansumali, I. V. Karlin, S. Arcidiacono, A. Abbas, and N. I. Prasianakis, Phys. Rev. Lett. **98**, 124502 (2007).

[12] S. Ansumali, I. V. Karlin, and H. C. Öttinger, Europhys. Lett. **63**, 798 (2003).

[13] G. R. McNamara, A. L. Garcia, and B. J. Alder, J. Stat. Phys. **81**, 395 (1995).

[14] X. W. Shan, X. Yuan, and H. Chen, J. Fluid Mech. **550**, 413 (2006).

[15] D. N. Siebert, L. A. Hegele, and P. C. Philippi, Phys. Rev. E **77**, 026707 (2008).
[16] I. V. Karlin, S. S. Chikatamarla, and S. Ansumali, Comm. Comp. Phys. **2**, 196 (2007).
[17] S. Ansumali and I. V. Karlin, J. Stat. Phys. **107**, 291 (2002).
[18] S. Chapman and T. G. Cowling, *The Mathematical Theory of Non-Uniform Gases* (Cambridge University Press, Cambridge, UK, 1970).
[19] X. B. Nie, X. Shan, and H. Chen, Europhys. Lett. **81**, 34005 (2008).
[20] P. J. Dellar, in *Computational Fluid and Solid Mechanics*, edited by K.-J. Bathe (2005), pp. 532–635.
[21] G. R. McNamara, A. L. Garcia, and B. J. Alder, J. Stat. Phys. **87**, 1111 (1997).
[22] R. A. Brownlee, A. N. Gorban, and J. Levesley, Phys. Rev. E **75**, 036711 (2007).
[23] H. Chen and X. W. Shan, Physica D **237**, 2003 (2008).
[24] S. S. Chikatamarla and I. V. Karlin, Comput. Phys. Commun. **179**, 140 (2008).
[25] S. S. Chikatamarla, S. Ansumali, and I. V. Karlin, Phys. Rev. Lett. **97**, 010201 (2006).
[26] I. V. Karlin, A. G. Tomboulides, C. E. Frouzakis, and S. Ansumali, Phys. Rev. E **74**, 035702(R) (2006).
[27] S. S. Chikatamarla, Ph.D. thesis, Swiss Federal Institute of Technology (ETH), Zurich, 2008 (unpublished).